

Three Dimensional Raman Cooling using Velocity Selective Rapid Adiabatic Passage

Axel Kuhn, H       Perrin, Wolfgang H       and Christophe Salomon
*Laboratoire Kastler Brossel,        Normale Sup      ,
 24 rue Lhomond, 75231 Paris Cedex 05, France*

We present a new and efficient implementation of Raman cooling of trapped atoms. It uses Raman pulses with an appropriate frequency chirp to realize a velocity selective excitation through a rapid adiabatic passage. This method allows to address in a single pulse a large number of non zero atomic velocity classes and it produces a nearly unity transfer efficiency. We demonstrate this cooling method using cesium atoms in a far-detuned crossed dipole trap. Three-dimensional cooling of 1×10^5 atoms down to $2 \mu\text{K}$ is performed in 100 ms. In this preliminary experiment the final atomic density is $1.3 \times 10^{12} \text{ at/cm}^3$ (within a factor of 2) and the phase-space density increase over the uncooled sample is 20. Numerical simulations indicate that temperatures below the single photon recoil temperature should be achievable with this method.

Reference: OSA TOPS on Ultracold Atoms and BEC, Vol. 7 (Keith Burnett ed.) 1996, p.58

Key Words

Trapped atoms, Laser cooling, Ultracold atoms, Coherent optical effects

I. INTRODUCTION

The recent observation of Bose-Einstein condensation in dilute alkali vapors was a major advance in the field of atom cooling and trapping [1, 2]. The quantum degeneracy threshold was reached by evaporative cooling of the atomic sample in a magnetic trap. Despite the tremendous success of these experiments, one can see two important drawbacks to this method for future applications of these Bose condensates: (i) the strong magnetic field gradients required for the evaporation and their time dependence are not easily compatible with the high precision measurements of, for instance, cold atoms frequency standards and atom interferometers. (ii) The evaporation is relatively slow (tens of seconds), requires a very low rate of inelastic collisions and leads to a substantial loss of atoms (typically a factor 100). A possible route to solve both of these problems is to trap the atoms with optical fields and to apply to the trapped atoms the subrecoil cooling methods first developed for free atoms. Optical fields are easily switched on and off and, if properly designed, subrecoil cooling presents a priori no loss of atoms. Recently Raman cooling of trapped Na atoms has produced a sample at $1 \mu\text{K} = 0.42 T_R$, where $T_R = \hbar^2 k^2 / M k_B$ is the single photon recoil temperature [3]. This is a factor 320 increase in phase-space density but still a factor 300 short of the condensation threshold.

In this paper, we present a new Raman method for subrecoil cooling of trapped atomic samples and our efforts to reach the quantum degeneracy on atomic cesium by purely optical methods. Contrarily to previous demonstrations of Raman cooling, we use velocity selective Raman pulses in which both the amplitude and the frequency are changed in a controlled way. This produces a velocity selective rapid adiabatic passage which is very efficient (transfer efficiency close to one) and which can excite simultaneously a large number of velocity classes.

This paper is organized as follows: we first recall the main elements of Raman cooling (section II). We then describe the Rapid Adiabatic Passage (RAP), its velocity selectivity, and optimization of the frequency chirp to reach an efficiency close to one (section III). The effect of the pulse rate in the cooling sequence and of the atomic motion in a crossed dipole trap is studied using a numerical simulation of the cooling process for cesium atoms (section IV). The experimental setup is described in section V. The loading of the crossed dipole trap from a Magneto Optical Trap (MOT) and the results of Raman cooling using the RAP method are given in section VI.

II. RAMAN COOLING SCHEME

Raman cooling was first proposed for subrecoil cooling of free atoms in one dimension [4]. It has recently been used to cool cesium atoms down to a 1D temperature of $3 \text{ nK} = T_R/70$ [6]. Since in subrecoil cooling schemes, the temperature decreases with increasing interaction times [6, 7], the extension of the method to trapped atoms is very attractive because of the potentially long storage time [3]. In addition, in an harmonic trap, the phase space density scales as T^{-3} . In the trap, the cooling can be performed along a single axis because, under certain circumstances, the motion of the atoms couples all three degrees of freedom [3]. As we will show in section IV, this coupling causes new effects which lead to a different cooling strategy than for free atoms.

The principle of the cooling mechanism is shown in fig.1 in the case of cesium atoms. Two counter-propagating Raman pulses excite the atoms from $F = 3$ to $F = 4$ in the ground state $6^2S_{1/2}$ and push them by $2\hbar k$ towards zero velocity. One chooses the pulse shapes and detunings in a proper way to avoid excitation of atoms at rest and to select only the desired velocity class.

Subsequently, the excited atoms are brought back to the initial level $F = 3$ by pumping them to the excited $6^2P_{3/2}$ state which decays by spontaneous emission with a rate $\Gamma = 2\pi \times 5.3 \text{ MHz}$. We have chosen the $F = 3$ level in the excited state which decays with a branching ratio of $2/3$ to the initial state. To avoid a system-

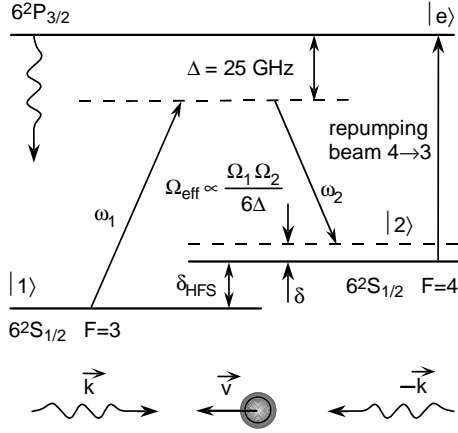


FIG. 1: Raman excitation scheme and subsequent repumping to $F = 3$ by excitation of $F = 4 \rightarrow 3$.

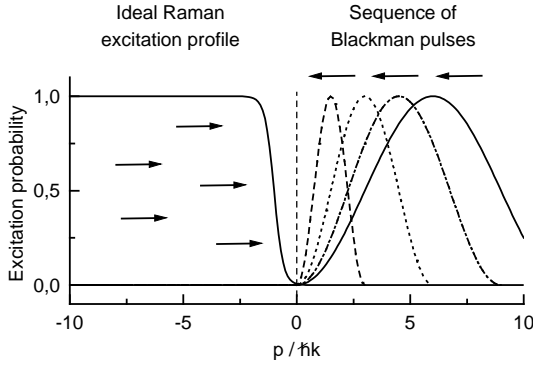


FIG. 2: Idealized Raman excitation profile (shown for $p < 0$) and traditionally realized pulses (for $p > 0$)

atic momentum transfer by this repumping process, the laser shines on the atoms in a molasses geometry. This repumping process communicates between two and four photons of random directions. There is no average momentum change in this process, but this dissipative random walk is required to reach sub-recoil temperatures. In addition, it produces some heating in the directions perpendicular to the Raman axis. One has to take this into account to optimize the cooling sequence (see section IV).

Usually, the initial momentum distribution is much larger than $\hbar k$ and the cooling relies on a repetition of the Raman- and repumping pulses. In fig.2, we show an *ideal* Raman excitation profile on the left-hand side. It provides an excitation probability of ‘one’ for all atoms at $p < -2\hbar k$ and tends towards zero around $p = 0$. Traditionally, such an ideal excitation profile was replaced by a sequence of Π -pulses at different detunings [3–6], starting at large Raman detuning δ and compressing the velocity distribution by a reduction of δ from pulse to pulse.

On free atoms, the direction of the Raman pulses is changed from pulse to pulse to cool both wings of the

initial velocity distribution. In a three dimensional trap, there is no need to alternate the Raman beam directions because the atoms oscillate in the harmonic potential. However, the dissipative repumping process and the oscillatory motion may bring some atoms to high velocities that are no more affected by the Raman pulse with the smallest detuning. Therefore, the sequence has to be restarted at higher detuning to re-collect these atoms. In fact, one single Raman pulse affects only a small fraction of the velocity distribution (especially the narrow band pulses at small δ). There are also some technical disadvantages of such a sequence. One has to fulfill the Π -pulse condition for each of them, and the pulse duration has to be adapted to δ to avoid the excitation of atoms at rest.

Most of the disadvantages of such a Π -pulse sequence vanish if one provides pulses with an ideal excitation profile in momentum space. In the following section, we demonstrate the usefulness of the well known rapid adiabatic passage (RAP) to tailor the desired Raman excitation profile.

III. RAPID ADIABATIC PASSAGE

The first successful combination of stimulated Raman scattering involving adiabatic passage in a Λ -type three level system by Bergmann [9] was based on time delayed Raman pulses with fixed frequencies. The excitation probability of such a scheme reflects the Fourier transform of the applied pulses. The same holds for the previous Raman cooling schemes using coinciding Blackman [4] or square pulses [6] with fixed frequencies at large detuning Δ .

In the latter case, the simplification of the three level system to an effective two level system is justified if $\Delta \gg |\Omega_{1,2}|$. In our method, we further allow the Raman detuning δ_{eff} to be time dependent. The interaction Hamiltonian is then

$$H_{\text{eff}}(t) = -\frac{\hbar}{2} \begin{pmatrix} 0 & \Omega_{\text{eff}}(t) \\ \Omega_{\text{eff}}^*(t) & 2\delta_{\text{eff}}(t) \end{pmatrix}. \quad (1)$$

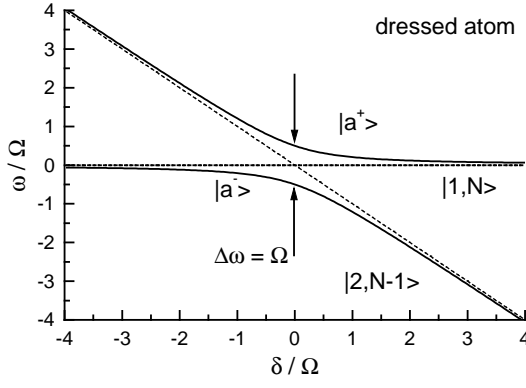
It describes the evolution of $|\Psi\rangle$ in the basis of the initial level $|1\rangle$ and final level $|2\rangle$, the intermediate level being eliminated. In this effective two level system, it is clear that rapid adiabatic passage (RAP), as described by Loy [8], can be employed when the Raman detuning δ_{eff} is chirped across the resonance.

If one takes into account the different magnetic sublevels m_F , the effective Rabi frequency and detuning read

$$\Omega_{\text{eff}} = \frac{\Omega_1 \Omega_2}{6\Delta} \sqrt{1 - \left(\frac{m_F}{4}\right)^2} \quad (2)$$

$$\delta_{\text{eff}} = \delta + \frac{\delta_{\text{HFS}}^2(\Omega_1^2 - \Omega_2^2) + \Delta \delta_{\text{HFS}}(\Omega_1^2 + \Omega_2^2)}{4\Delta(\Delta^2 - \delta_{\text{HFS}}^2)} \quad (3)$$

At this point, we note that it is impossible to have the same Π -pulse condition for all magnetic sublevels, because the effective Rabi frequencies depend on m_F . In

FIG. 3: Avoided crossing at $\delta = 0$

addition, because of the differential light shift, the effective detuning δ_{eff} depends on Ω .

In a dressed state picture, the eigenstates of the two state Hamiltonian read

$$\begin{aligned} |a^+\rangle &= \cos\phi|1\rangle - \sin\phi|2\rangle \\ |a^-\rangle &= \sin\phi|1\rangle + \cos\phi|2\rangle \end{aligned} \quad \tan\phi = \frac{\sqrt{\Omega^2 + \delta^2} - \delta}{\Omega}, \quad (4)$$

with the corresponding eigenfrequencies

$$\omega^\pm = -\frac{\delta}{2} \pm \frac{1}{2}\sqrt{\Omega^2 + \delta^2} \quad (5)$$

Both the mixing angle ϕ and the eigenfrequencies ω^\pm are a function of the Raman detuning δ . If δ sweeps across the resonance, ϕ turns from $\pi/2$ to 0 (which is valid for $\Omega \ll \delta$ in the wings of a Raman pulse), and by consequence $|a^-\rangle$ evolves from $|1\rangle$ to $|2\rangle$. In fig.3, the corresponding avoided crossing at $\delta = 0$ is shown.

If the extend of the frequency chirp is limited, only the atoms which experience such a crossing due to their Doppler shifted resonance frequency are excited by the Raman pulse. Even atoms which do not experience a crossing follow $|a^-\rangle$ adiabatically, but the dressed state returns to the initial state $|1\rangle$ in the end of the pulse.

In fig.4, the evolution of the eigenfrequencies of a real three level system is shown for a fixed frequency chirp and different Doppler shifts. (a) shows a crossing right in the center of the chirp, (b) shows that there is still an avoided crossing when the Doppler shift is close to the border of (but within) the chirp. If the Doppler shift coincides with the detuning in the end (c), $|a^+\rangle$ and $|a^-\rangle$ become degenerate and both states are equally populated. (d) shows that there is no more avoided crossing if the Doppler shifted resonance is not within the chirp, i.e. there is no Raman excitation in such a case and no momentum exchange takes place. In fact, the extend of the chirp determines the range of velocities which are excited.

A. Shape of the δ chirp

To insure that the state vector $|\Psi\rangle$ follows the dressed state $|a^-\rangle$ adiabatically throughout the interaction, the

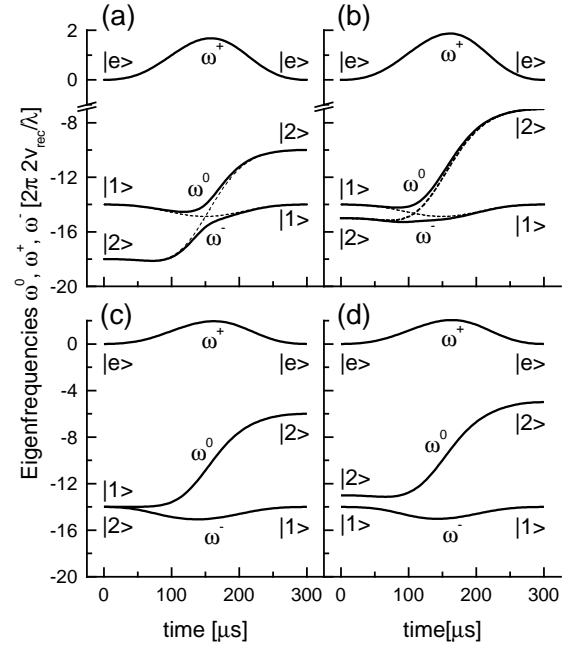


FIG. 4: Energies of the dressed levels (solid lines) in response to a frequency chirped Blackman pulse with a duration of 300 μs and a pulse area $\int \Omega(t)dt = 3\pi$. The dashed lines represent the energies of the uncoupled states. The chirp extends from $\delta = -24 kv_{\text{rec}}$ to $\delta = -6 kv_{\text{rec}}$. Due to the Doppler shift $\delta_{\text{eff}} = \delta_{\text{chirp}} + 2kv$ of the counter-propagating Raman beams, atoms in the velocity interval $-12 \lesssim v/v_{\text{rec}} \lesssim -3$ are affected. The evolution is shown for four different initial velocities – (a): $v/v_{\text{rec}} = -7.5$; (b): $v/v_{\text{rec}} = -4$; (c): $v/v_{\text{rec}} = -3$; (d): $v/v_{\text{rec}} = -2$.

adiabaticity criterion (see [10])

$$|\langle a^+ | \frac{d}{dt} | a^- \rangle| \ll |\omega^+ - \omega^-| = \sqrt{\Omega^2 + \delta^2}, \quad (6)$$

needs to be fulfilled. It is most stringent in the vicinity of the crossing, where it can be expressed as

$$\left| \frac{d}{dt} \delta \right| \ll \Omega^2. \quad (7)$$

Due to the different atomic velocities, the exact position of the crossing within the chirp is not known. Therefore the chirp has to be shaped like

$$\delta(t) \propto \int \Omega^2(t)dt, \quad (8)$$

to insure the same adiabaticity condition for all atoms. The chirp thus reflects the pulse shape and is fast at high Rabi frequencies and slow at small Ω . Fig.5 shows the shape of the Raman pulse together with the optimized chirp.

B. Efficiency and Selectivity

A straightforward numerical simulation of the RAP excitation was done solving the time-dependent

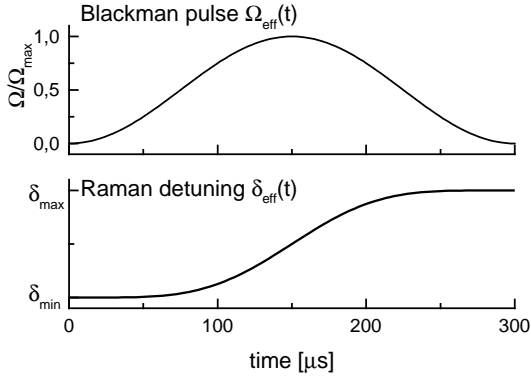


FIG. 5: Form of the Blackman shaped Raman pulse (upper part) and the superimposed frequency chirp (lower part).

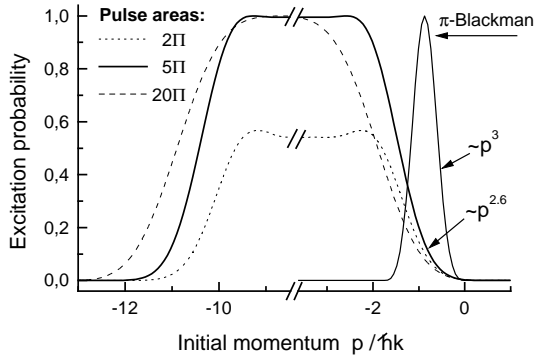


FIG. 6: Transfer efficiency of frequency chirped Raman pulses in comparison with the excitation profile of a non-chirped Blackman pulse. All pulses have a duration of 300 μs and are chirped by $\Delta\delta = 2\pi \times 74$ kHz, which extends over 9 v_{rec} . The start frequency is shifted from resonance in order to avoid exciting atoms at rest. Also shown is the power law dependence of the excitation profiles near $p = 0$.

Schrödinger equation. We show the resulting transfer efficiency as a function of the atomic velocities (i.e. the Doppler shift) for different pulse amplitudes in fig.6. The simulation shows that a box-like excitation profile is realized with such pulses, but it reveals at the same time that the border of the profile is not as steep as the one achieved with a Blackman pulse of same duration.

Once the recoil limit $p \lesssim \hbar k$ is reached, a description of the cooling process using Lévy flight statistics [11] shows that there is an ideal exponent α for the excitation probability $P_{\text{exc}} \propto v^\alpha$ around $v = 0$. It depends on the dimension D of the cooled atomic ensemble and

$$\frac{D}{\alpha} = \mu \lesssim 1 \quad (9)$$

is the optimal choice for free atoms [6]. There is no real ‘zero’ in the excitation profile of the chirped Raman pulses and one has to choose an arbitrary cut-off to determine the origin. If one chooses $P_{\text{exc}} t_{\text{trap}} \Gamma_{\text{cool}} = 0.25$ as condition to determine this origin (i.e. a probability of 25% to excite atoms at rest during the trap-

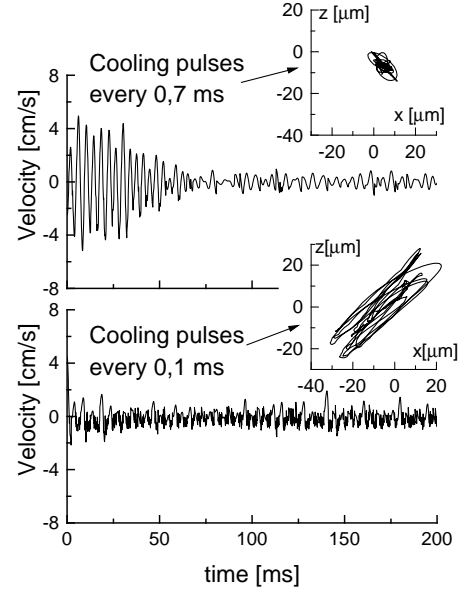


FIG. 7: Time evolution of the velocity component along the Raman axis for different pulse rates Γ_{cool} . Projections of the corresponding trajectories (between 100 ms and 200 ms) in the plane containing the vertical and the Raman axis are shown in the insets.

ping time t_{trap}). We obtain for a typical cooling time $t_{\text{trap}} = 200$ ms, a cooling pulse rate $\Gamma_{\text{cool}} = 0.5$ ms and pulse parameters of fig.6:

$$\alpha_{\text{RAP}} \simeq 2.6. \quad (10)$$

In this case, D/α is slightly greater than one, which is not the optimum choice to enter far in the subrecoil region. By contrast, a Blackman pulse without frequency chirp has a first minimum in its excitation profile where $\alpha_{\text{BM}} \simeq 3.3$ is well determined. Therefore, a combination of both profiles, a chirped Blackman at large detuning and a narrow fixed frequency Blackman pulse might turn out to be the optimum choice.

IV. COOLING SEQUENCE

In three dimensional Raman Cooling, one has to be aware that the re-thermalization after each pulse has to take place. We call Γ_{therm} this thermalization rate and Γ_{couple} the rate of coupling of the atomic motion to the Raman axis. If the pulse rate Γ_{cool} in the cooling sequence is larger than both of these rates, i.e. if

$$\Gamma_{\text{cool}} > \max(\Gamma_{\text{therm}}, \Gamma_{\text{couple}}), \quad (11)$$

the coupling of the atomic motion perpendicular to the Raman axis to this same axis becomes ineffective. In such a case, the ensemble is cooled in one dimension at the expense of heating the other degrees of freedom due to the dissipative repumping process.

The Monte Carlo simulation of single atom trajectories in fig.7 demonstrates this effect. We have calculated 3D

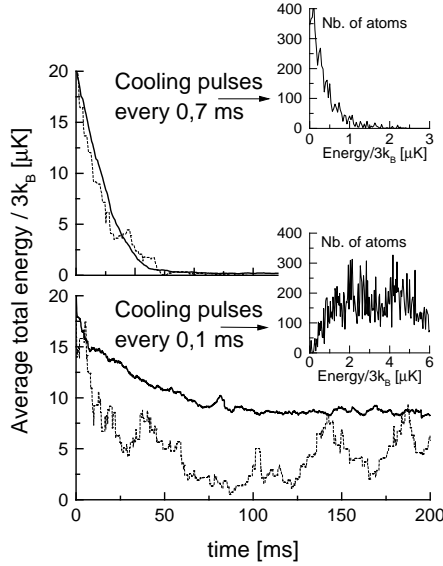


FIG. 8: Total energy loss for different pulse rates Γ_{cool} . The solid lines show the average over 100 atoms, the dashed lines correspond to single trajectories. In the insets are shown the energy distributions in the steady-state.

classical trajectories with random initial positions and velocities and have chosen a simplified excitation profile for the Raman pulses:

$$P_{\text{exc}}(p) = \begin{cases} 1 & p < -3\hbar k \\ |p/3\hbar k|^2 & \text{for } -3\hbar k \leq p \leq 0 \\ 0 & p > 0 \end{cases} \quad (12)$$

In the simulation, every $\Gamma_{\text{cool}}^{-1}$ the atom can be excited according to P_{exc} . Once a Raman excitation takes place, the repumping process is simulated by adding three momenta $\hbar k$ of random directions.

For the different cooling rates shown in fig.7, the velocity component along the Raman axis decreases in all cases. However, a closer look to the trajectory for the high cooling rate $\Gamma_{\text{cool}}^{-1} = 0.1$ ms reveals that the other degrees of freedom are not cooled efficiently.

The energy loss due to the different cooling rates in fig.8 underline this effect. After 100 ms, an equilibrium is reached in case of a high pulse rate, i.e. the heating of the perpendicular motion is balanced by the combination of cooling and coupling to the Raman axis. The ‘temperature’ of 9 μK is rather high in this case (there is no thermal distribution – we express the average energy in terms of a ‘temperature’). On the other hand, the low cooling rate $\Gamma_{\text{cool}}^{-1} = 0.7$ ms allows an effective coupling of the atomic motion to the Raman axis. A simulation of the temperature obtained after a typical cooling time $t_{\text{trap}} = 200$ ms is shown in fig.9 as function of $\Gamma_{\text{cool}}^{-1}$. Due to the limited cooling time, there is an optimum choice $\Gamma_{\text{cool}}^{-1} = 0.7$ ms for which the temperature reaches 0.2 μK , i.e. the recoil temperature for cesium. At lower pulse rates, the number of pulses is too small to bring the temperature further down. We have observed that

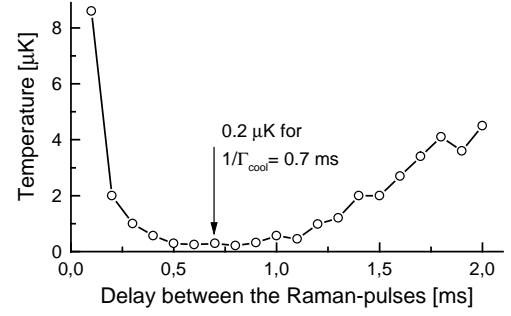


FIG. 9: Temperature reached after 100 ms Raman cooling as a function of the pulse rate.

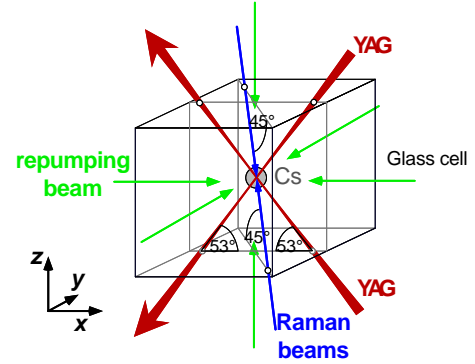


FIG. 10: Configuration of the dipole and Raman beams.

for cooling times longer than 200 ms, the temperature still decreases below 200 nK.

V. EXPERIMENTAL SETUP

A. YAG and Raman beams

Atoms are loaded in the crossed dipole trap from a vapor cell magneto optical trap (MOT) [13]. The beam configuration of the red detuned dipole trap is shown in fig.10. We use a 1064 nm TEM₀₀ Nd:YAG laser which is split into two arms having each a power of 7 W. These two beams cross in their focal points with a common waist $w_0 = 80 \mu\text{m}$. Both of them propagate in a vertical plane and make an angle of $\pm 37^\circ$ with the vertical.

The attractive potential (see fig.11) is caused by the ground state light shift

$$\Delta E = \frac{\hbar \Omega_{\text{YAG}}^2(\vec{r})}{4\Delta_{\text{YAG}}} \quad (13)$$

and corresponds to a well depth of 150 μK . With these laser parameters, gravity is compensated only in the intersection volume of the two beams. Because of the large detuning of the YAG laser, the maximum photon scattering rate at the center of the trap is 3 s^{-1} . The calculated oscillation frequencies near the bottom of the potential

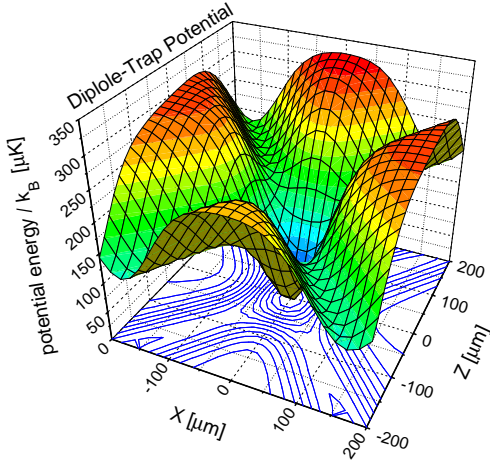


FIG. 11: Cut of the dipole trap potential in the plane of the beams.

are

$$\nu_x = 458 \text{ Hz} \quad \nu_y = 577 \text{ Hz} \quad \nu_z = 350 \text{ Hz}, \quad (14)$$

where x and y design the directions in the horizontal plane, y being perpendicular to both of the dipole beams, and z the vertical axis.

The Raman cooling beams are spatially filtered using optical fibers and propagate along the (1,1,1) direction referred to the eigen-axes of oscillation in the dipole trap. This provides an effective coupling of the one dimensional cooling to all degrees of freedom of the atomic motion. The waist of the Raman beams is on the order of ~ 1 mm and their power is up to 35 mW. For a detuning $\Delta = 2\pi \times 25$ GHz, the maximum effective Rabi frequency is $\Omega_{\text{eff}} = 4 \times 10^5 \text{ rad.s}^{-1}$. The two beams are issued from two diode lasers whose frequency difference is phase-locked to a stable frequency source at the 9.2 GHz Cesium hyperfine frequency [5, 6]. The shape, central frequency and frequency chirp of the pulses are achieved using acousto-optic modulators. The Raman transfer from $F = 3$ to $F = 4$ is followed by a repumping pulse, resonant with the $F = 4 \rightarrow F' = 3$ transition which returns the atoms to $F = 3$. This repumping laser illuminates the atoms in a six beam molasses geometry (fig.10).

B. Detection

We measure the atom number, the velocity distribution of the trapped atoms and the size of the cloud: the number of atoms and the velocity distribution are deduced from fluorescence measurements while the size is obtained by absorption imaging [2]. After switching off the YAG beams, we turn on a σ^+ polarized probe beam tuned to the $F = 4 \rightarrow F' = 5$ transition which overlaps the dipole trap. It is slightly red detuned and in a standing wave configuration. 2% of the fluorescence light is collected with a lens on a calibrated photodiode. For

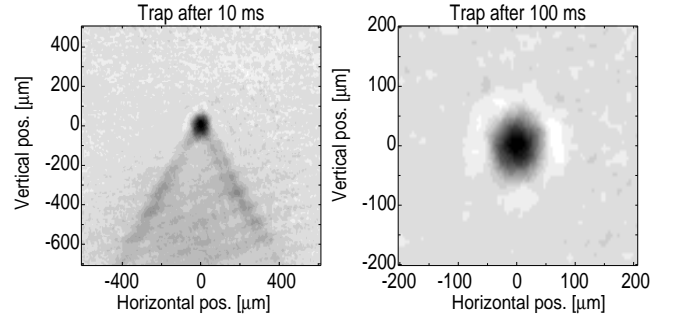


FIG. 12: Absorption images of cesium atoms in the crossed trap in the lin⊥lin configuration of the YAG beams. After 100 ms, 10^5 atoms remain in the ‘harmonic’ trap and form a cloud of Gaussian shape with $\sigma_{x,y} \simeq 24 \mu\text{m}$, $\sigma_z \simeq 30 \mu\text{m}$.

measuring the momentum distribution, we use velocity selective Raman transition [12]. We transfer a narrow velocity class from $F = 3$ to $F = 4$ with a $200 \mu\text{s}$ Blackman Π -pulse. The fluorescence of these selected atoms is then recorded as above. By scanning the Raman detuning δ we obtain the full momentum distribution, with a resolution of about $\hbar k/2$.

The absorption image is obtained on a CCD camera by shining a $15 \mu\text{s}$ probe beam pulse on the trapped atoms in the (1,1,0) direction (in the horizontal plane). The probe is typically detuned by -1.5Γ from resonance. The trap is imaged with a magnification of 4 on the CCD. The image appears as the ratio between a picture with atoms and a reference picture without atoms. The absorption picture gives the size of the trap with a resolution of about $8 \mu\text{m}$ and an independant measure of the number of atoms.

VI. EXPERIMENTAL RESULTS

A. Loading the Dipole Trap

Cesium atoms are first collected for 1 s in the MOT from the background gas at 10^{-9} mbar. In order to capture the largest possible number of atoms, the YAG trap and the MOT overlap in time for about 100 ms. Within this time, the MOT is contracted by doubling the magnetic field gradient to 30 Gauß/cm and reducing the intensity of the MOT beams by a factor of 20 to 1 mW/cm^2 . The detuning of the beams is increased to -10Γ for a short period (~ 5 ms) to further cool the atoms before switching the MOT off. Absorption images recorded 10 ms and 100 ms after switching off the MOT are shown in fig.12. After 10 ms the atoms initially at the intersection of the YAG beams remain trapped while the others fall preferentially along the YAG beams. After 100 ms, 10^5 atoms (1% of the number of atoms in the MOT) remain in the crossed dipole trap with a density of $3 \times 10^{11} \text{ atoms/cm}^3$ (within a factor 2) and an initial temperature of $6 \mu\text{K}$.

We have observed that the loading of the YAG trap and

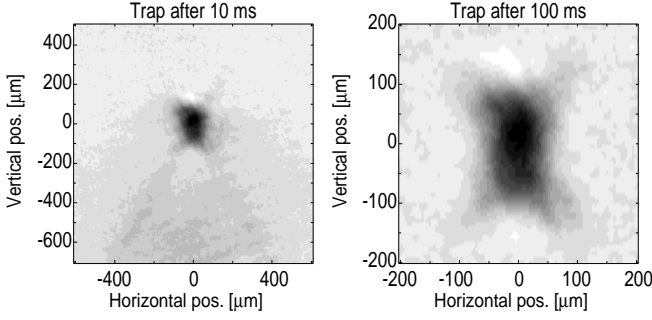


FIG. 13: Absorption images in the lin||lin configuration of the YAG beams. The X shape of the trap which contains 5×10^5 atoms is due to an intensity modulation along the vertical (see text).

the shape of the atomic cloud was strongly dependent of the polarization of the YAG beams. When the two YAG beams have linear and parallel polarizations, the number of trapped atoms is about 5 times higher than in the case of orthogonal polarizations. The shape of the cloud (fig.13) is also very different as it displays a 'X' pattern. We attribute this effect as being due to the intensity interference pattern along the vertical when the two polarizations are parallel. This produces horizontal planes of micro-wells on the scale of the YAG wavelength ($\lambda_{\text{YAG}}/2 \sin 53^\circ$). The atoms are trapped in these planes of intensity maxima and the effective trapping volume is larger. An interesting application of this interference effect might be to enhance the loading efficiency of the YAG trap. After loading with parallel polarizations we could rotate the polarization of one of the beams during the cooling phase to collect these atoms in the bottom of the harmonic trap.

When the YAG beams have linear and orthogonal polarizations, there is no intensity modulation but there is a polarization lattice along z which leads to a modulation of the light shift potential. It is easy to show that both of the cesium D1 and D2 transitions (at 894 nm and 852 nm respectively) contribute to the light shift in a way which depends on the local polarization. The amplitude of the modulation is proportional to the frequency difference between the D1 and D2 lines and is opposite for the $F = 3$ and $F = 4$ hyperfine states. It represents about $\pm 10\%$ of the total depth of the potential. Because our YAG laser has several longitudinal modes, this polarization lattice may fluctuate in time and produce an unwanted heating.

B. Realization of the Raman excitation profile

To realize the optimal excitation profile, we first note that the effective detuning of the Raman transition depends on the power of the Raman beams as given by eq.(3).

For $\Delta > \delta_{\text{HFS}}$ it is not possible to cancel the light shift term in eq.(3), so that the instantaneous resonance frequency is shifted proportionally to the instantaneous

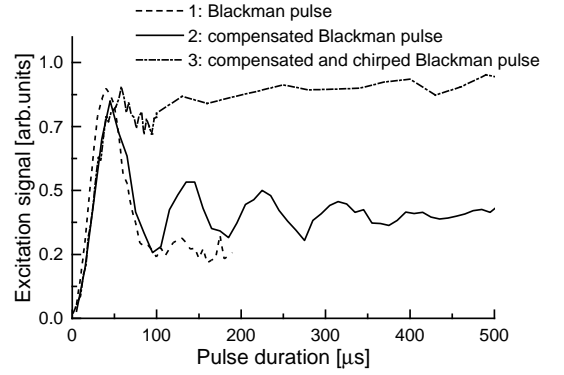


FIG. 14: Excitation rate as a function of the pulse duration; intensity is kept constant; (1) Blackman pulse without light shift compensation; (2) Blackman pulse with light shift compensation; (3) chirped Blackman pulse for rapid adiabatic passage (including light shift compensation).

intensity of the pulse. This leads to an imperfect π -pulse condition and to a damping of Rabi oscillations when using Blackman pulses as shown in fig.14, curve 1.

In order to solve this problem, we actively compensate the light shift by chirping the detuning during the Blackman pulse. Several periods of the Rabi oscillation in time become then visible (fig.14, curve 2). The effective Rabi frequency can be measured by this method and for instance fig.14 gives $\Omega_{\text{eff}} = 7 \times 10^4$ rad/s. The 'damping' of the oscillation is mostly due to the interference between the various m -dependent Rabi frequencies (See eq.(2a)). In the case of the pulses used for the rapid adiabatic passage which are frequency chirped, we add the compensation of the light shift to the RAP chirp. In such conditions and with a frequency chirp symmetric around resonance (fig.14, curve 3), the excitation probability remains close to one for a pulse area greater than 3π .

We then tested the efficiency of the rapid adiabatic passage with copropagating Raman beams for which there is no velocity selectivity. The transfer efficiency as a function of Raman detuning δ is presented in fig.15 for a 200 μs long Blackman pulse chirped from -81 kHz to 0, $\Delta = 2\pi \times 25$ GHz and for various intensities. The agreement with theory (fig.6) is excellent. Note the high transfer efficiency (90%) and the square shape of the excitation profile for the pulse of area 5.7π which we will use in the Doppler sensitive case for Raman cooling (next section).

C. Raman cooling sequence

For Raman cooling, we use the Raman beams in the counter-propagating geometry. The transition probability of fig.15 becomes a Doppler sensitive excitation profile: for an atom with velocity v along the Raman beams, $\delta_{\text{eff}} = \delta + 2kv$. We carefully adjust the initial detuning and the pulse spectral width in order to avoid any ex-

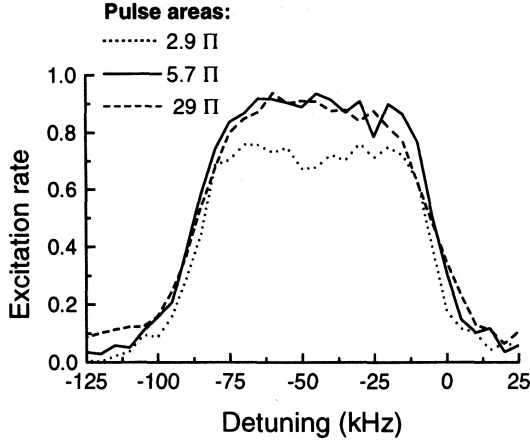


FIG. 15: Excitation probability as a function of detuning for 200 μ s Blackman pulses chirped from -81 kHz to 0; the three curves correspond to three different pulse areas.

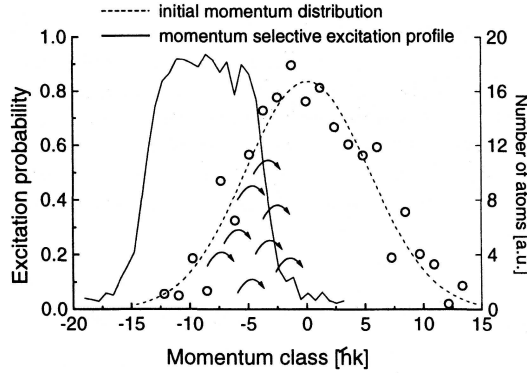


FIG. 16: Measured initial momentum distribution in the crossed dipole trap ($T = 5.6 \mu$ K) and Doppler selective excitation profile for a 200 μ s long chirped Blackman pulse.

citation at zero velocity. Fig.16 shows the momentum dependent excitation profile of a 200 μ s Blackman pulse chirped over 81 kHz together with the initial momentum distribution. We optimize the cooling sequence to get the narrowest momentum distribution after a fixed time (70 ms). We find that the temperature of the cooled atoms is larger if the pulse rate is too high. This observation is in agreement with the simple simulation described in section IV. The optimal cooling sequence was: a 300 μ s Blackman pulse exciting the atoms with momentum between $-12\hbar k$ and $-3\hbar k$, followed by a 100 μ s repumping pulse. The total time between two cooling pulses was then 400 μ s, which corresponds to 7 to 10 pulses per oscillation period. This sequence was repeated 170 times.

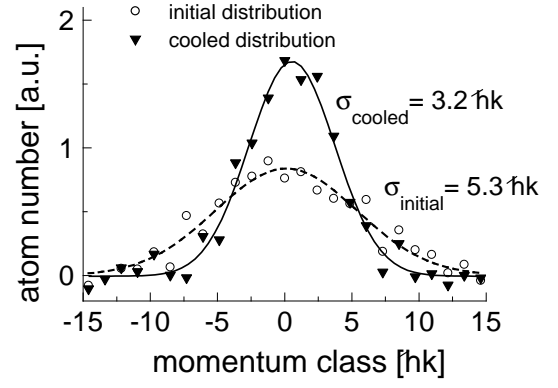


FIG. 17: Momentum distribution before and after Raman cooling.

D. Results

The result of the Raman cooling is shown in fig.17: before cooling, the momentum distribution along the Raman axis is gaussian with a $\sigma = 5.3\hbar k$ dispersion. We were able to cool the atomic sample down to $\sigma = 3.2\hbar k$. This corresponds to a temperature of $T = 2.0 \mu$ K. Since the areas of the two momentum distributions are equal, there is no atom loss during the cooling process.

The momentum dispersion along one axis was reduced by a factor $\eta = 1.65$. The increase in phase space density, proportional to η^6 for atoms trapped in a harmonic potential, is a factor 20. We also checked that the cooling was effective in 3 dimensions by taking absorption pictures of the trap before and after cooling with the CCD camera. The density of the cooled atoms is $1.3 \times 10^{12} \text{ cm}^{-3}$ with an uncertainty of a factor 2.

E. Limitations and prospects

For longer cooling sequences, we did not reach a temperature smaller than 2 μ K. Nor was the temperature lower when we added a second, longer, pulse in order to excite atoms with momentum between $-3\hbar k$ and $-1\hbar k$. We suspect that Raman cooling is in competition with a residual heating mechanism due to a time dependent interference between the YAG beams inducing fluctuations of the trapping potential. A possible solution to this problem is to alternate in time the two YAG trapping beams at a rate much higher than the oscillation frequencies. Our numerical simulations indicate that, after suppression of this heating, temperatures near the single photon recoil temperature should be accessible. Such a value would be near the Bose-Einstein condensation threshold, if we neglect possible density limitations due to photon multiple scattering [14, 15]. A second interesting development is to initiate evaporative cooling from the high density already obtained in this dipole trap [16].

Acknowledgments

We gratefully acknowledge C.Cohen-Tannoudji, J.Dalibard, J.Reichel, E.Peik, M.Ben Dahan and Y.Castin for stimulating discussions. A. K. is indebted

to the Alexander von Humboldt-Stiftung for support. This work was supported in part by CNES, NEDO and Collège de France. Laboratoire Kastler Brossel is Unité de recherche de l'Ecole Normale Supérieure et de l'Université Pierre et Marie Curie, associée au CNRS.

-
- [1] M.H.Anderson, J.R.Ensher, M.R.Matthews, C.E.Wieman and E.A.Cornell, *Science* **269**, 198 (1995)
 - [2] K.B.Davis, M.-O.Mewes, M.R.Andrews, N.J. van Druten, D.S.Durfee, D.M.Kurn, and W.Ketterle, *Phys.Rev.Lett.* **75**, 3969 (1995)
 - [3] H.J.Lee, C.S.Adams, M.Kasevich and S.Chu, *Phys.Rev.Lett.* **76**, 2658 (1996)
 - [4] M.Kasevich and S.Chu, *Phys.Rev.Lett.* **69**, 1741 (1992)
 - [5] J.Reichel, O.Morice, G.M.Tino and C.Salomon, *Europhys.Lett.* **28**, 477 (1994)
 - [6] J.Reichel, F.Bardou, M. Ben Dahan, E.Peik, S.Rand, C.Salomon and C.Cohen-Tannoudji, *Phys.Rev.Lett.* **75**, 4575 (1995)
 - [7] A.Aspect, E.Arimondo, R.Kaiser, N.Vansteenkiste and C.Cohen-Tannoudji, *Phys.Rev.Lett.* **61**, 826 (1988)
 - [8] M.M.T.Loy, *Phys.Rev.Lett.* **32**, 814 (1974)
 - [9] U.Gaubatz, P.Rudecki, S.Schiemann and K.Bergmann, *J.Chem.Phys.* **92**, 5363 (1990); S.Schiemann, A.Kuhn, S.Steuerwald and K.Bergmann, *Phys.Rev.Lett.* **71**, 3637 (1993)
 - [10] A.Messiah, *Mécanique Quantique*, Vol.2, Chap.17, Dunod, Paris (1959)
 - [11] F.Bardou, J.P.Bouchaud, O.Emile, A.Aspect and C.Cohen-Tannoudji, *Phys.Rev.Lett.* **75**, 4575 (1995); P.Lévy, *Théorie de l'Addition des Variables Aléatoires*, Gautier-Villars (1954)
 - [12] M.Kasevich and S.Chu, *Phys.Rev.Lett.* **67**, 181 (1991)
 - [13] C.Monroe, W.Swann, H.Robinson et C.Wieman, *Phys.Rev.Lett.* **65**, 1571 (1990)
 - [14] M.Olshanii, Y.Castin and J.Dalibard, *Proc. Laser Spectr.* XII, 7 (1995)
 - [15] J.I.Cirac, M.Lewenstein and P.Zoller, *Europhys.Lett.* **35**, 647 (1996)
 - [16] C.S.Adams, H.J.Lee, N.Davidson, M.Kasevich and S.Chu, *Phys.Rev.Lett.* **74**, 3577 (1995)